Compton scattering from 6Li at 60 MeV

L. S. Myers,[1] M. W. Ahmed,[1,2] G. Feldman,[3] S. S. Henshaw,[1] M. A. Kovash,[4] J. M. Mueller,[1] and H. R. Weller[1]

[1]*Department of Physics and Triangle Universities Nuclear Laboratory, Duke University, Box 90308, Durham, North Carolina 27708, USA*
[2]*Department of Physics, North Carolina Central University, Durham, North Carolina 27707, USA*
[3]*Department of Physics, George Washington University, Washington, DC 20052, USA*
[4]*Department of Physics and Astronomy, University of Kentucky, Lexington, Kentucky 40506, USA*

Compton scattering cross sections from 6Li have been measured at scattering angles of $40°–160°$ using a nearly monoenergetic 60-MeV photon beam at the High Intensity Gamma-Ray Source. A phenomenological model provides an estimate of the sensitivity of the $^6\text{Li}(\gamma, \gamma)^6\text{Li}$ cross section to the nucleon isoscalar electromagnetic polarizabilities α_s and β_s.

PACS number(s): 25.20.Dc

I. INTRODUCTION

During the past thirty years, much effort has been devoted to measuring and understanding the electromagnetic polarizabilities, α and β, of the proton and neutron. These polarizabilities are the first-order responses of the nucleon's internal structure to an applied electric or magnetic field. The efforts have been very successful in the case of the proton but less so for the neutron.

The majority of the attempts to measure the nucleon polarizabilities have utilized nuclear Compton scattering. In the limit where the photon energy is much lower than the pion production threshold, the Compton scattering cross section of a nucleon can be written as [1]

$$\frac{d\sigma}{d\Omega} = \left(\frac{d\sigma}{d\Omega}\right)_{\text{Born}} - \frac{q^2}{4\pi M}\left(\frac{\omega'}{\omega}\right)^2(\omega\omega')$$
$$\times \left\{\frac{\alpha+\beta}{2}(1+\cos\theta)^2 + \frac{\alpha-\beta}{2}(1-\cos\theta)^2\right\}, \quad (1)$$

where q and M are the nucleon charge and mass, ω and ω' are the energies of the incident and scattered photons, θ is the photon scattering angle in the laboratory frame, and $(d\sigma/d\Omega)_{\text{Born}}$ is the Born cross section for a nucleon with an anomalous magnetic moment [2]. Terms of $O(\omega^3)$ and higher have been dropped in this cross-section expansion. The forward-angle cross section is dominated by the contribution from $\alpha + \beta$ while the backward-angle cross section is most sensitive to $\alpha - \beta$. Furthermore, the sum of the polarizabilities is constrained by the Baldin sum rule [3]:

$$\alpha + \beta = \frac{1}{2\pi^2}\int_{\omega_{th}}^{\infty}\frac{\sigma_\gamma(\omega)d\omega}{\omega^2}, \quad (2)$$

where $\sigma_\gamma(\omega)$ is the total photoabsorption cross section of the nucleon and ω_{th} is the energy of the pion photoproduction threshold.

Several Compton scattering experiments near and below the pion production threshold have been performed on the proton over the years [4–8], with the most recent global fit [9] to all the data up to 170 MeV yielding values of

$$\alpha_p = 10.7 \pm 0.3_{\text{stat}} \pm 0.2_{\text{BSR}} \pm 0.8_{th},$$
$$\beta_p = 3.1 \mp 0.3_{\text{stat}} \pm 0.2_{\text{BSR}} \pm 0.8_{th}, \quad (3)$$

where the statistical errors are shown as well as the errors due to uncertainties in the Baldin sum rule (BSR) and the theory. The units of α and β are 10^{-4} fm^3. These results were obtained under the constraint of the current evaluation [8] of the Baldin sum rule for the proton, which is

$$\alpha_p + \beta_p = 13.8 \pm 0.4. \quad (4)$$

The current global fit of the neutron polarizabilities is much less precise. Compton scattering measurements directly off the neutron are not possible due to the lack of a free neutron target. As such, experimenters have had to resort to using light nuclei such as 2H [10–13], 4He [14], 12C [15–19], and 16O [18–21] to try to measure α_n and β_n. The results for the heavier nuclei are ambiguous due to uncertainties in the model parametrizations. Current models based on effective field theory [9] are able to extract nucleon polarizabilities from $^2\text{H}(\gamma, \gamma)^2\text{H}$ but the data suffer from relatively large statistical errors. Using the deuteron Compton scattering data, the polarizabilities have been determined to be [9]

$$\alpha_n = 11.1 \pm 1.8_{\text{stat}} \pm 0.4_{\text{BSR}} \pm 0.8_{th},$$
$$\beta_n = 4.1 \mp 1.8_{\text{stat}} \pm 0.4_{\text{BSR}} \pm 0.8_{th} \quad (5)$$

under the Baldin sum-rule constraint for the neutron [22]:

$$\alpha_n + \beta_n = 15.2 \pm 0.4. \quad (6)$$

The exact values of α and β are critical for testing how accurately the theory describes physics accessible only in the two-photon response (e.g., Compton scattering) of the nucleon. Their extraction also provides a nontrivial benchmark of our understanding of charged meson-exchange currents in light nuclei [9]. Additionally, recent work [23] has indicated that the largest source of uncertainty in the evaluation of the proton-neutron mass difference is related to the isovector magnetic polarizability, $\beta_p - \beta_n$. The current values of the proton and neutron polarizabilities are equal within the errors listed; however, better statistical errors are needed in order to determine α_n and β_n more precisely and to provide a more stringent test of the theory.

To that end, we have carried out a Compton scattering measurement on 6Li, the first since Pugh *et al.* [24]. 6Li was chosen because it is expected to have a Compton scattering

cross section almost an order of magnitude larger than that of ^{2}H. At sufficiently low energies (below ~100 MeV), the photon scattering is coherent and the total scattering amplitude is simply the sum of the individual Thomson amplitudes for the Z protons in the target nucleus [9]:

$$R(E, \theta) \sim \frac{Ze^2}{m}, \tag{7}$$

which implies that the cross section scales as Z^2.

Current models are not able to make precise predictions for Compton scattering cross sections for ^{6}Li, but, as Orlandini notes [25], various theoretical approaches are now starting to make progress in predicting observables in higher-mass (i.e., $A \geqslant 3$) nuclei. While we will not extract particular values for the polarizabilities, we will attempt to demonstrate the sensitivity of the ^{6}Li$(\gamma, \gamma)^6$Li scattering cross section to α and β using a phenomenological model.

II. EXPERIMENTAL SETUP

In this paper, we report a measurement of the ^{16}O$(\gamma, \gamma)^{16}$O reaction cross section and a precision measurement of ^{6}Li$(\gamma, \gamma)^6$Li at 60 MeV. The ^{16}O cross section is well known and serves the purpose of gauging the systematic uncertainty of the absolute cross-section determination for the ^{6}Li data. The present measurements were conducted at the High Intensity Gamma-Ray Source (HI$\vec{\gamma}$S) facility [26] at Triangle Universities Nuclear Laboratory (TUNL). The HI$\vec{\gamma}$S facility is capable of producing high-intensity, nearly monoenergetic, ~100% polarized γ rays. For this measurement the beam was circularly polarized. The quasi-monoenergetic nature of the γ-ray beam significantly reduces the background as compared to the earlier Compton measurements, which were conducted using bremsstrahlung-produced beams. The HI$\vec{\gamma}$S beam results in less background in the detected energy spectrum, making the extraction of the photon yield more reliable.

The HI$\vec{\gamma}$S facility utilizes a free-electron laser to produce γ rays via Compton backscattering. The γ-ray beam passes through a collimator which defines the radius of the beam and determines the intensity and energy spread of the incident γ rays. For this experiment, the 60-MeV γ-ray beam had an energy spread of ~4.5% and an on-target intensity of ~10^7 γ/s [27]. The collimated beam is incident on a five-scintillator-paddle system [28] which detects recoil electrons and positrons from photoelectric, Compton, and pair-production processes and has been directly calibrated using a 25.4-cm-diameter, 35.6-cm-long NaI(Tl) detector. The five-scintillator-paddle system provides a means of measuring the instantaneous γ-ray intensity without creating a source of background radiation in the experiment. After the intensity monitor, the γ rays are incident on the scattering target (either ^{6}Li or ^{16}O) and some are Compton scattered into one of eight large-volume NaI(Tl) detectors. The detectors were placed at roughly equally spaced angles from 40° to 160°, as shown in Fig. 1.

Each NaI(Tl) detector core measures approximately 25.4 cm in diameter and 30.5 cm long. Surrounding the core detector is a segmented NaI(Tl) annular detector that is 7.5 cm thick and 30.5 cm long and is designed as an
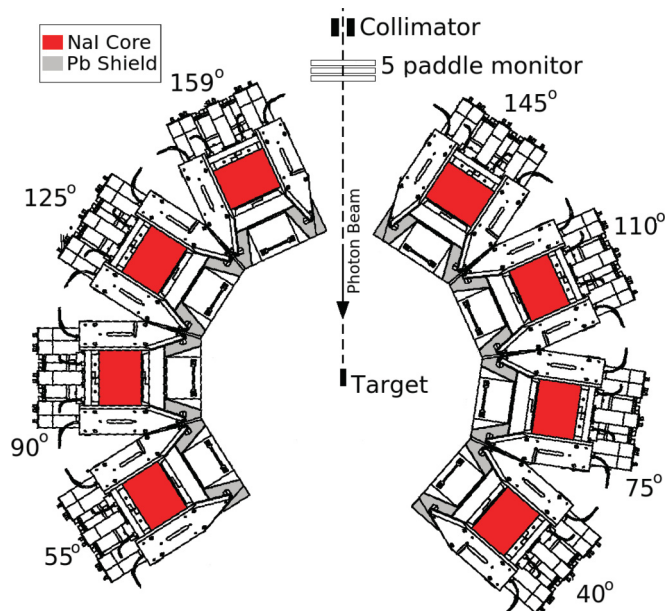

FIG. 1. (Color online) Schematic diagram (not to scale) of the experimental layout showing the arrangement of the NaI(Tl) detectors.

anticoincidence shield. The detector-response line shapes from the core detectors had a full width at half maximum of ~6% at 60 MeV (see Fig. 2), part of which (~4.5%) is due to the energy spread of the incident γ-ray beam. Lead shielding was placed surrounding the front face of each detector to reduce backgrounds and define the scattering solid angle. Each detector was placed so that the solid angle subtended by the aperture in the lead shield was ~45 msr. The aperture was filled with borated wax to eliminate neutron backgrounds in the core with minimal effect on the photon energy resolution.

The oxygen target consisted of distilled water in a Lucite cylinder 10.0 cm long and 5.0 cm in diameter, yielding an oxygen target thickness of 10.0 ± 0.1 g/cm^2. The contribution to the scattering yield due to the target end caps was determined to be less than 1%. The ^{6}Li target was produced at the University of Saskatchewan [29]; the target cell consists of
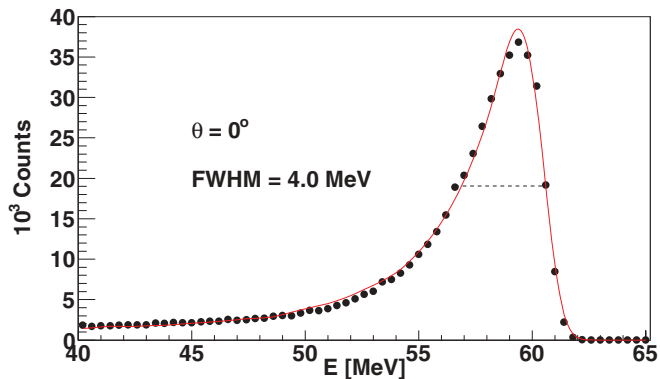

FIG. 2. (Color online) Energy spectrum from a NaI(Tl) detector with the γ-ray beam directed into the detector ($\theta = 0°$). The full width at half maximum is 4.0 MeV (6.7%). The solid line is the fit to this spectrum using a GEANT4 simulation.

a polyvinyl chloride (PVC) cylinder with PVC and Al foil end caps. It measures 12.7 cm in length with a diameter of 4.1 cm for a target thickness of 5.84 ± 0.06 g/cm^2. Since the scattering contribution from the cell was estimated to be $\sim 2\%$, a measurement of photon scattering from an empty cell was performed. An identical empty target cell was prepared and placed in the beam in order to determine the background contribution from the target end caps.

III. DATA ANALYSIS

Data were read out from each detector into a charge-to-digital converter (QDC), which can be converted into photon energy, and a time-to-digital converter (TDC), which enables coincident timing. The pulsed nature of the photon beam at HI$\vec{\gamma}$S provides a very clean TDC prompt peak in each of the eight NaI(Tl) detectors (Fig. 3). At the time of this run, the anticoincidence shields were nonoperational, which resulted in the flat, uncorrelated (random) background appearing in the timing spectrum due to non-beam-related sources such as cosmic rays.

QDC spectra for prompt and random events were filled by placing cuts on the prompt peak and a suitable random window in the TDC spectrum. The prompt window contains both true scattered photons and some fraction of the random events. By setting a wide random window, the net true spectrum can be defined as

$$S_{net} = S_{prompt} - \frac{W_{prompt}}{W_{random}} \times S_{random}, \quad (8)$$

where S_{net}, S_{prompt}, and S_{random} are the net, prompt, and random energy spectra, and W_{prompt} and W_{random} represent the widths of the prompt and random windows. For the ^{6}Li data, the empty-target data were analyzed in the same manner as the full target (see Fig. 4). The empty-target spectrum is then subtracted from the full-target spectrum after being properly normalized to the number of incident photons on target. The yield of the empty target in the elastic peak region (defined as 55 to 61.5 MeV) was $< 2\%$ of the yield in the full target. Typical final detector-response line shapes are shown for ^{6}Li (Fig. 5) at both forward and backward scattering angles. The low-energy background in the forward-angle detector is assumed to be coming from forward-peaked, atomic scattering events in the target. The backward-angle detectors do not see this background.
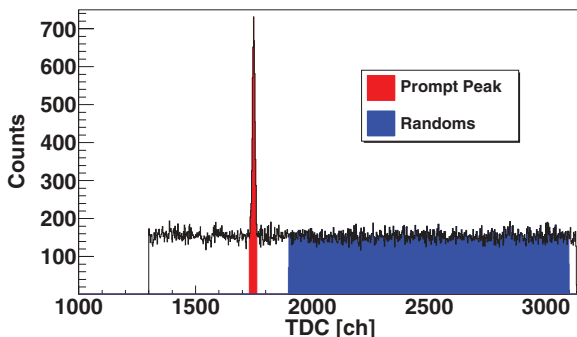

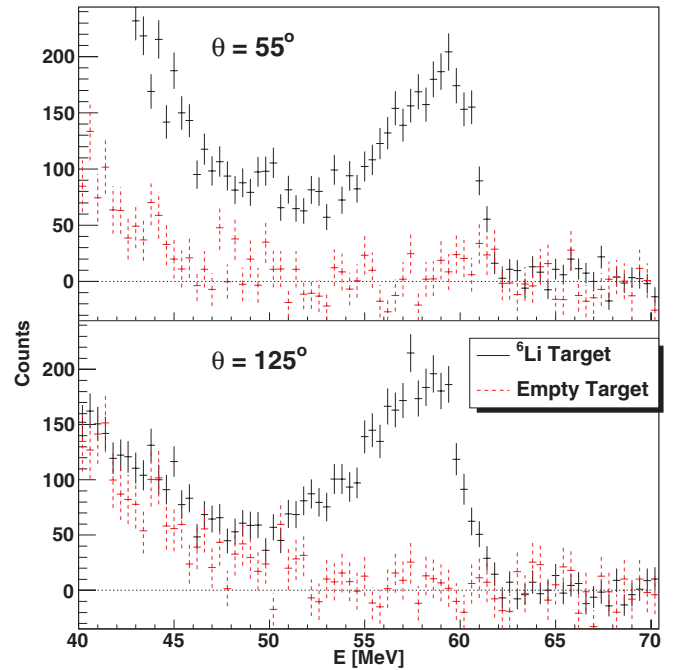FIG. 3. (Color online) TDC spectrum from a NaI(Tl) detector. The prompt and random windows are shown.

FIG. 4. (Color online) The net true energy spectra for the full (^{6}Li) and empty targets at $\theta = 55°$ and $125°$. The spectra have been normalized to the number of incident photons on target.

GEANT4 [30] was employed to determine the total line shape yield and also to make any corrections due to finite geometry effects. The simulation output was first determined for the case of the NaI(Tl) detector positioned directly in the beam line ($\theta = 0°$) as seen in Fig. 2. The intrinsic simulation was smeared with a Gaussian function to account for the characteristics of each NaI(Tl) detector that are difficult to model in GEANT4. The simulated detector response, with the smearing fixed as above, is then fit to the scattering data over a region of interest (ROI) that extended over a range of 6.5 MeV as indicated in Fig. 5. It is critical that the summing window not extend into the low-energy background in the forward-angle detectors. This background was taken into account as an exponential function, as shown in the top panel of Fig. 5. The summing window was chosen so that the background contribution was minimal to reduce any systematic uncertainties related to the modeling. The background contribution was found to be less than 1% in the summing window. The fitted GEANT4 line shape is used to correct for the detection efficiency of the NaI(Tl) detector in the ROI; this efficiency accounts for events that deposit some energy outside the ROI in the detector. Additionally, the correction factor for photons absorbed by the target and the correction to the solid angles due to the finite geometry of the experimental setup are obtained from the simulation.

The first excited state of ^{16}O is at 6.05 MeV above the ground state so, based on the ROI defined above, inelastic scattering from this state is not expected to contribute to the elastic yield. However, in the case of ^{6}Li, there are several excited states within 5.65 MeV of the ground state. In order to determine whether inelastic scattering from any of these states contributed to the elastic peak, the data were fit with two GEANT4 simulated line shapes. The first line shape was taken
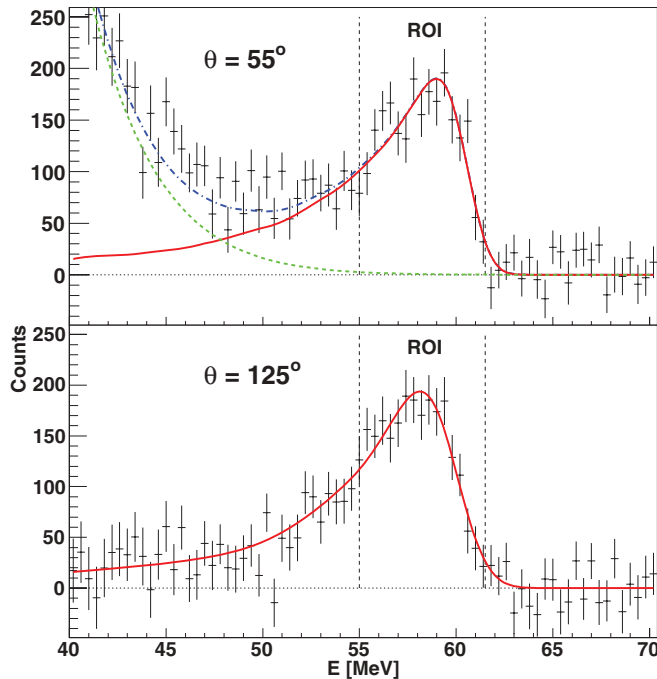
FIG. 5. (Color online) The net true energy spectra (with empty-target subtraction) at forward and backward angles for ^{6}Li. The region of interest (ROI) has been marked. (Top) At forward angles, the fit to the data (dashed-dotted line) is given by a sum of a low-energy background (dashed line) and a GEANT4 simulation (solid line). (Bottom) At backward angles, the only contribution is from the GEANT4 simulation (solid line).

as the elastic peak and the second line shape was assumed to result from the first excited state at 2.19 MeV in ^{6}Li. The relative strength of these two line shapes was varied in order to fit the data. The inelastic contribution is expected to be largest at the most backward angle (i.e., highest momentum transfer).
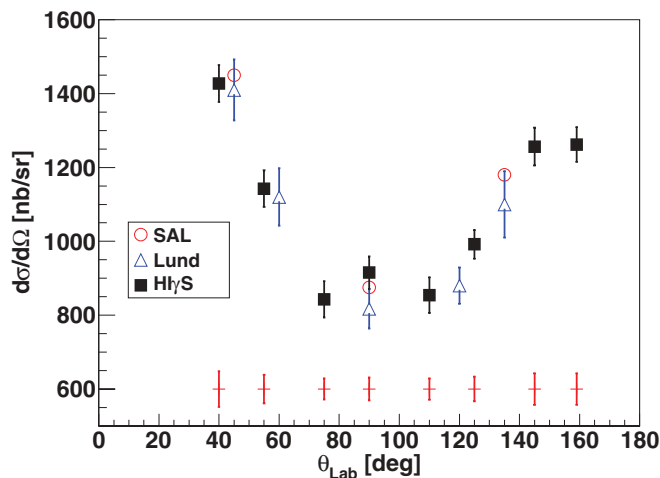

FIG. 6. (Color online) Comparison of scattering cross section of ^{16}O obtained by [18,19] and [20,21] and current results. Statistical errors are shown on the data points. Systematic errors for this measurement are shown under the data by the red bars. The 90° data point from SAL/Illinois is an extrapolation based on measurements taken at higher energies [21].
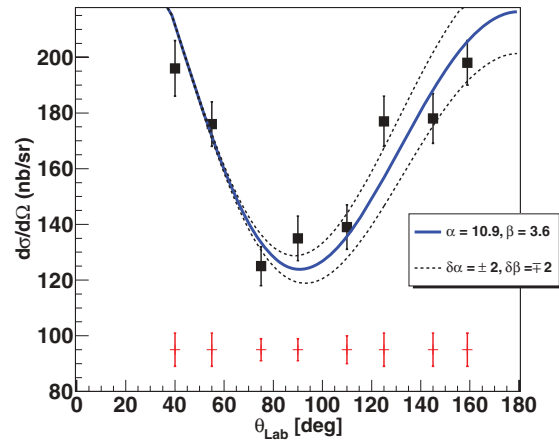

FIG. 7. (Color online) The scattering cross section of ^{6}Li from this experiment. Statistical errors are shown on the data points. Systematic errors for this measurement are shown under the data by the red bars. The curves are results from fitting the data to a phenomenological model.

The quality of the fit to the data at $\theta = 159°$ decreases as the inelastic strength is increased. When the χ^2 value has increased by 1.0 (68% confidence limit) from the value obtained by assuming only an elastic peak, a maximum contribution of inelastic scattering to the ROI yield of 6% can be set. Since there is no conclusive evidence that the inelastic contribution must be incorporated, it has been ignored in the extraction of the cross section.

The cross sections are plotted as a function of laboratory scattering angle in Fig. 6 for ^{16}O and in Fig. 7 for ^{6}Li. Figure 6 shows the previous ^{16}O data from Lund [18,19] and the Saskatchewan Accelerator Laboratory (SAL) and University of Illinois collaboration [20,21]. The Lund data were collected at 58 MeV and the SAL/Illinois data at 60 MeV. The agreement is very good between the current data and these published measurements. This result gives confidence that the absolute cross-section extraction does not suffer from any unknown systematic effects.

There are no such high-quality data to compare to the present ^{6}Li cross-section results. Based on the cross sections of other light nuclei and the Z^2 dependence of the Compton scattering cross section, the estimated average ^{6}Li$(\gamma, \gamma)^6$Li cross section should be on the order of 150 nb/sr [31]. The data are certainly consistent with this estimate, as seen in Fig. 7.

TABLE I. Compton scattering cross sections of ^{16}O and ^{6}Li at $E_\gamma = 60$ MeV. The first error is statistical and the second is systematic.

θ_{Lab}	^{16}O $\frac{d\sigma}{d\Omega}$ (nb/sr)	^{6}Li $\frac{d\sigma}{d\Omega}$ (nb/sr)
40°	$1427 \pm 50 \pm 48$	$196 \pm 10 \pm 6$
55°	$1143 \pm 50 \pm 39$	$176 \pm 8 \pm 6$
75°	$843 \pm 49 \pm 29$	$125 \pm 7 \pm 4$
90°	$915 \pm 44 \pm 31$	$135 \pm 7 \pm 4$
110°	$854 \pm 48 \pm 29$	$139 \pm 8 \pm 5$
125°	$992 \pm 39 \pm 34$	$177 \pm 9 \pm 6$
145°	$1256 \pm 51 \pm 43$	$178 \pm 9 \pm 6$
159°	$1262 \pm 47 \pm 43$	$198 \pm 8 \pm 6$

The extracted cross sections for ^{16}O and ^{6}Li are given in Table I along with the statistical and systematic errors. The systematic errors are dominated by the uncertainty in the number of incident photons on target (2.0%) and the solid angle (2.4%).

IV. PHENOMENOLOGICAL MODEL

A phenomenological model has been used to evaluate the sensitivity of the ^{6}Li data to the magnitude of the electromagnetic polarizabilities. This model is based on the work presented in [15] and [21]. The Compton scattering amplitude can be written in terms of the one- and two-body seagull (SG) amplitudes, which are explicitly dependent on the isoscalar polarizabilities, $\alpha_s = (\alpha_p + \alpha_n)/2$ and $\beta_s = (\beta_p + \beta_n)/2$, as [21]

$$
\begin{aligned}
R(E, \theta) = {} & R^{GR}(E, \theta) + R^{QD}(E, \theta) \\
& + R_1^{SG}(E, \theta) + R_2^{SG}(E, \theta).
\end{aligned} \tag{9}
$$

The first two terms in Eq. (9) are related to the giant resonances (GR) and the quasideuteron (QD) process, respectively. The amplitudes are given by

$$
\begin{aligned}
R^{GR}(E, \theta) = {} & f_{E1}(E) g_{E1}(\theta) + f_{E2}(E) g_{E2}(\theta) \\
& + \frac{NZ}{A} r_0 [1 + \kappa_{GR}] g_{E1}(\theta)
\end{aligned} \tag{10}
$$

and

$$
R^{QD}(E, \theta) = \left[f_{QD}(E) + \frac{NZ}{A} r_0 \kappa_{QD} \right] F_2(q) g_{E1}(\theta), \tag{11}
$$

where the complex forward scattering amplitudes $f_\lambda(E)$ ($\lambda = E1$, $E2$, QD) are taken to have a Lorentzian form [32] given by

$$
\mathfrak{Re} f_\lambda(E) = \frac{E_\lambda^2 - E^2}{4\pi\hbar c} \frac{1}{\Gamma_\lambda} \frac{\sigma_\lambda E^2 \Gamma_\lambda^2}{\left(E^2 - E_\lambda^2\right)^2 + E^2 \Gamma_\lambda^2} \tag{12}
$$

and

$$
\mathfrak{Im} f_\lambda(E) = \frac{E}{4\pi\hbar c} \frac{\sigma_\lambda E^2 \Gamma_\lambda^2}{\left(E^2 - E_\lambda^2\right)^2 + E^2 \Gamma_\lambda^2}, \tag{13}
$$

where E_λ, Γ_λ, and σ_λ are the resonance energy, width, and strength, respectively. Also in Eqs. (10) and (11), the appropriate angular factor is $g_\Lambda(\theta)$ (see Tables II and III), r_0 is the classical nucleon radius, and the enhancement factors $[1 + \kappa_{GR}]$ and κ_{QD} are the integrals of the GR and QD photoabsorption cross sections in units of the classical dipole sum rule. Since the QD process is modeled as an interaction with a neutron-proton pair, it is modulated by a two-body form factor $F_2(q)$, where q is the momentum transfer.

TABLE II. Dipole and quadrupole angular factors.

Λ	$g_\Lambda(\theta)$
$E1$	$\vec{\epsilon} \cdot \vec{\epsilon}'$
$M1$	$(\vec{\epsilon} \times \hat{k}) \cdot (\vec{\epsilon}' \times \hat{k}')$
$E2$	$(\vec{\epsilon} \cdot \vec{\epsilon}')(\hat{k} \cdot \hat{k}') + (\vec{\epsilon} \cdot \hat{k}')(\vec{\epsilon}' \cdot \hat{k})$

TABLE III. Dipole and quadrupole angular interference factors.

$\Lambda \Lambda'$	$g_\Lambda(\theta)\, g_{\Lambda'}(\theta)$
$E1E1, M1M1$	$(1 + \cos^2\theta)/2$
$E1M1$	$\cos\theta$
$E1E2$	$\cos^3\theta$
$M1E2$	$(3\cos^2\theta - 1)/2$
$E2E2$	$(1 - 3\cos^2\theta + 4\cos^4\theta)/2$

The seagull amplitudes account for subnucleon and meson-exchange degrees of freedom and are necessary to preserve gauge invariance in the total scattering amplitude. The one-body seagull amplitude is

$$
\begin{aligned}
R_1^{SG}(E, \theta) = {} & -F_1(q) \Bigg\{ \left[Z r_0 - \left(\frac{E}{\hbar c} \right)^2 A \alpha_s \right] g_{E1}(\theta) \\
& - \left[\left(\frac{E}{\hbar c} \right)^2 A \beta_s \right] g_{M1}(\theta) \Bigg\},
\end{aligned} \tag{14}
$$

where higher-order terms have been omitted. This process is modulated by the one-body form factor $F_1(q)$, which is taken to be [33]

$$
\begin{aligned}
F_1(q) = {} & \rho_0 \frac{4\pi}{3} R_p^3 \frac{\pi c_p q}{\sinh(\pi c_p q)} \frac{3}{q R_p} \\
& \times \left[\frac{\sin(q R_p)}{(q R_p)^2} \frac{\pi c_p q}{\tanh(\pi c_p q)} - \frac{\cos(q R_p)}{q R_p} \right],
\end{aligned} \tag{15}
$$

where, under the normalization $F_1(0) = 1$,

$$
\rho_0^{-1} = \frac{4\pi}{3} R_p^3 \left[1 + \left(\frac{\pi c_p}{R_p} \right)^2 \right] \tag{16}
$$

and $R_p = 1.77$ fm and $c_p = 0.327$ fm are given by the two-parameter Fermi function parametrization of the charge distribution [34]:

$$
\rho(r) = \frac{\rho_0}{1 + e^{\frac{r - R_p}{c_p}}}. \tag{17}
$$

The two-body seagull amplitude is

$$
R_2^{SG}(E, \theta) = -F_2(q) \frac{NZ}{A} (\kappa_{GR} + \kappa_{QD}) r_0 g_{E1}(\theta), \tag{18}
$$

where higher-order terms have been dropped. The two-body form factor is chosen by convention as $F_2(q) = [F_1(q/2)]^2$.

V. RESULTS

Due to a lack of detailed knowledge of the giant resonance structures of ^{6}Li to serve as inputs to the model, it is not possible to extract accurate values of the polarizabilities. However, this phenomenological model is still able to provide insight into the *sensitivity* of the ^{6}Li(γ, γ)^{6}Li cross section to α_s and β_s. Initially we fixed the polarizabilities to $\alpha_s = 10.9$ and $\beta_s = 3.6$ as listed in [9] and then allowed the resonance parameters to vary until the fit is optimized. Since this experiment was carried out at an energy above any presumed resonance energy, it is sensitive only to the integral

TABLE IV. $E1$, $E2$, and QD parameters for ^{6}Li. Values marked with an asterisk have been determined by fitting.

Contribution	E_{res}(MeV)	Γ_{res}(MeV)	σ_{res}(mb)
$E1$	25.0	12.0	7.2*
$E2$	34.0	16.0	0.14*
QD	40.0	100	1.1

of the resonance and not the details of its shape (i.e., its width and energy). As such, the resonance locations have been fixed at 25 and 34 MeV for the $E1$ and $E2$ resonances, and the widths were set to 12.0 and 16.0 MeV. The QD parameters have been fixed to the values listed in [19]. The resonance amplitudes obtained from the fit are listed in Table IV along with the fixed parameters, and the resulting cross section is shown as the solid curve in Fig. 7. The energy-weighted sum-rule exhaustions are $\sim$75% ($E1$) and $\sim$60% ($E2$).

The sensitivity of the data to the polarizabilities can be observed by systematically varying α_s and β_s. The polarizabilities were each varied by ±2 units under the constraint that $\alpha_s + \beta_s = 14.5$, consistent with the average of the sum rules in Eqs. (4) and (6). As seen by the dashed lines in Fig. 7, this variation provides some estimate of the uncertainty in α_s and β_s. This relationship can be determined more rigorously by fitting α_s and β_s to the data in order to determine the error bars of that fit. In this case, we fix all the resonance parameters to the values in Table IV and then allow α_s and β_s to vary. This procedure results in a minor adjustment of α_s and β_s to 10.5 and 4.0, respectively. The effect of this modification of the polarizabilities is to slightly raise the back-angle cross section, which is expected because of the larger value of β_s. The resulting uncertainties in α_s and β_s based on this fit ($\delta\alpha_s^{stat} = \delta\beta_s^{stat} = 0.7$) are comparable to the global results presented in [9] ($\delta\alpha_s^{stat} = \delta\beta_s^{stat} = 0.9$) based on deuterium data. These error bars for ^{6}Li were obtained with only 50 h of beam time on target.

Due to the uncertainty in the resonance parameters and the inherent difficulty in unambiguously extracting the polarizabilities (as detailed in some previous measurements of light nuclei), it is not possible to make a quantitative statement about the accuracy or precision of the extraction of α_s and β_s using the phenomenological model. However, the indications are that with an accurate theoretical treatment of the ^{6}Li$(\gamma, \gamma)^6$Li reaction, this data set is capable of improving upon the current statistical errors of the isoscalar polarizabilities.

The results of this measurement are intended to spur further work on theoretical models of the ^{6}Li$(\gamma, \gamma)^6$Li reaction (e.g., the Lorentz integral transform method described in [35]) in order to precisely extract the isoscalar polarizabilities. A precision theoretical model should include the possible contribution from inelastic scattering since this experiment is
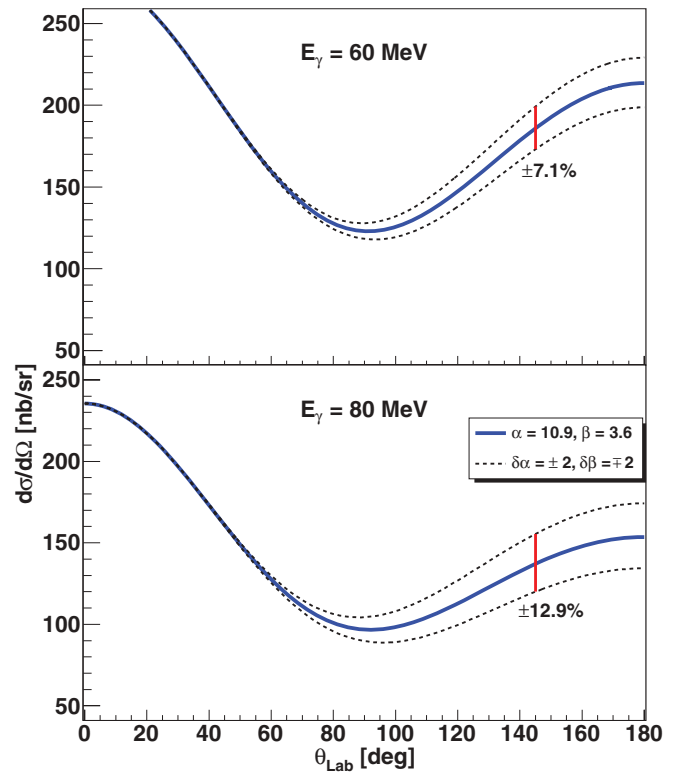

FIG. 8. (Color online) Scattering cross sections at 60 MeV (top) and 80 MeV (bottom) as predicted by the phenomenological model.

only able to rule out inelastic contributions at the 6% level. In addition, a subsequent measurement of this reaction is planned at HI$\vec{\gamma}$S at $E_\gamma \sim 80$ MeV, where the sensitivity of the cross section to the polarizabilities is expected to be greater than with the data presented here. At 80 MeV, the cross section drops by about 30% at back angles (see Fig. 8); however, the sensitivity is expected to increase by a factor of nearly 2. Given modest improvements in beam intensity, target size, or beam time on target, the statistics on the 80-MeV data set would be comparable to the data presented here. This future data set should further enhance the ability of a theoretical model to accurately extract the polarizabilities.

[1] V. A. Petrun'kin, Fiz. Elem. Chastits At. Yadra **12**, 692 (1981) [Sov. J. Part. Nucl. **12**, 278 (1981)].

[2] J. L. Powell, Phys. Rev. **75**, 32 (1949).

[3] A. M. Baldin, Nucl. Phys. **18**, 310 (1960).

[4] F. J. Federspiel *et al.*, Phys. Rev. Lett. **67**, 1511 (1991).

[5] A. Zieger *et al.*, Phys. Lett. B **278**, 34 (1992).

[6] E. L. Hallin *et al.*, Phys. Rev. C **48**, 1497 (1993).

[7] B. E. MacGibbon, G. Garino, M. A. Lucas, A. M. Nathan, G. Feldman, and B. Dolbilkin, Phys. Rev. C **52**, 2097 (1995).

[8] V. Olmos de Leon *et al.*, Eur. Phys. J. A **10**, 207 (2001).

[9] H. W. Grießhammer, J. A. McGovern, D. R. Phillips, and G. Feldman, Prog. Part. Nucl. Phys. **67**, 841 (2012).

[10] M. A. Lucas, Ph.D. thesis, University of Illinois at Urbana-Champaign, Champaign, IL, 1994.

[11] D. L. Hornidge *et al.*, Phys. Rev. Lett. **84**, 2334 (2000).

[12] M. Lundin *et al.*, Phys. Rev. Lett. **90**, 192501 (2003).

[13] L. S. Myers, Ph.D. thesis, University of Illinois at Urbana-Champaign, Champaign, IL, 2010.

[14] S. Proff *et al.*, Nucl. Phys. A **646**, 67 (1999).

[15] D. H. Wright, P. T. Debevec, L. J. Morford, and A. M. Nathan, Phys. Rev. C **32**, 1174 (1985).

[16] K. P. Schelhaas *et al.*, Nucl. Phys. A **506**, 307 (1990).

[17] B. J. Warkentin *et al.*, Phys. Rev. C **64**, 014603 (2001).

[18] M. Ludwig *et al.*, Phys. Lett. B **274**, 275 (1992).

[19] D. Häger *et al.*, Nucl. Phys. A **595**, 287 (1995).

[20] K. E. Mellendorf, Ph.D. thesis, University of Illinois at Urbana-Champaign, Champaign, IL, 1993.

[21] G. Feldman *et al.*, Phys. Rev. C **54**, 2124 (1996).

[22] M. I. Levchuk and A. I. L'vov, Nucl. Phys. A **674**, 449 (2000).

[23] A. Walker-Loud, C. E. Carlson, and G. A. Miller, Phys. Rev. Lett. **108**, 232301 (2012).

[24] G. E. Pugh, R. Gomez, D. H. Frisch, and G. S. Janes, Phys. Rev. **105**, 982 (1957).

[25] G. Orlandini, Eur. Phys. J. Spec. Top. **198**, 239 (2011).

[26] H. R. Weller *et al.*, Prog. Part. Nucl. Phys. **62**, 257 (2009).

[27] Y. K. Wu (private communication).

[28] R. E. Pywell, O. Mavrichi, W. A. Wurtz, and R. Wilson, Nucl. Instrum. Methods Phys. Res., Sect. A **606**, 517 (2009).

[29] W. A. Wurtz, Technical Report, University of Saskatchewan, http://nucleus.usask.ca/technical_reports/other/li_cast.pdf, (2007).

[30] S. Agostinelli *et al.*, Nucl. Instrum. Methods Phys. Res., Sect. A **506**, 250 (2003).

[31] G. Feldman *et al.*, HI$\vec{\gamma}$SProposal P08-10 Compton Scattering from ^{6}Li, 2010.

[32] R. Leicht *et al.*, Nucl. Phys. A **362**, 111 (1981).

[33] W. M. Alberico and A. Molinari, Z. Phys. A **309**, 143 (1982).

[34] C. W. De Jager, H. De Vries, and C. De Vries, At. Data Nucl. Data Tables **14**, 479 (1974).

[35] G. Bampa, W. Leidemann, and H. Arenhövel, Phys. Rev. C **84**, 034005 (2011).